J Solid State Electrochem (1998) 2: 170–175

ORIGINAL PAPER

Mahmoud M. Khader · Mahmoud M. Saleh
Emad M. El-Naggar

Photoelectrochemical characteristics of ferric tungstate

Received: 16 July 1997 / Accepted: 26 September 1997

Abstract Active ferric tungstate was prepared by fusing an equimolar mixture of tungsten oxide and ferric oxide at 1100 °C and annealing at 800 °C for 20 h. Analysis of the electrode material by X-ray diffraction showed that its composition was Fe_2WO_6. When this material was illuminated by visible light in 0.1 M NaOH solution, an anodic photocurrent at a positive potential of 0.5 V (SCE) was obtained. Therefore, this material is considered as an n-type semiconductor. The d.c. conductivity of this material at 25 °C was 4×10^{-6} Ω^{-1} cm^{-1}. In the dark, unexpectedly high anodic currents were observed at positive potentials of 0.8 V (SCE) in 0.1 M NaOH. These currents are attributed to the existence of a high density of electron-hole recombination centers within the band-gap of ferric tungstate. When dimethyl viologen (DMV) was used as an electroactive compound in the electrolyte, the anodic photocurrents increased significantly. The oxidation of DMV is thus expected to compete with the electron-hole recombination process. Furthermore, the process of electron-hole recombination was also predicted from the shape of the photocurrent transients under interrupted illumination. These transients exhibited first-order relaxation effects in the region of the onset time of the photocurrents. The band-gap energy of Fe_2WO_6 was found to be about 1.5 eV and its flat-band potential in 0.1 M NaOH was about −0.3 V (SCE). The photoelectrochemical properties of ferric tungstate are explained according to the formalism of the band model of the semiconductor/electrolyte interface.

Key words Photoelectrochemical · Ferric tungstate

M.M. Khader (✉) · M.M. Saleh · E.M. El-Naggar
Chemistry Department, Faculty of Science,
Cairo University, Cairo-Egypt

Introduction

In the last two decades, a great deal of research has been devoted to the study of electron transfer at illuminated semiconductor electrodes. One of the aims of this research was to make possible the use of such electrodes as half cells in electrochemical photo-voltaic cells [1–5]. It is recognized that three phenomena prevent practical application of such cells:

1. Small band-gap electrodes undergo corrosion anodically or cathodically in aqueous solutions as a result of photocurrent flow [6–10].
2. On the other hand, although wide band-gap semiconductors are known to be stable under illumination, they have the disadvantage of absorbing small portions of solar light.
3. Another important criterion is the thermodynamic incompatibility of the energy levels of the conduction and valence bands of the semiconductor at its surface with respect to the redox potentials of the electrolyte [11, 12].

The above phenomena have been studied extensively, and several promising suggestions for overcoming problems of photocorrosion have been put forward in the literature [13–17]. However, problems caused by the width of the band-gap and/or positions of the energy levels of a semiconductor at its surface with respect to the redox potentials of an electrolyte make it difficult to find convenient solutions. Studies of alternative semiconductors have been carried out in order to reach the required conditions of active photoelectrodes. Among these are studies of transition metal oxides. While simple oxides, e.g. TiO_2 and Fe_2O_3, have been extensively studied [11, 18–20], compound oxides, e.g. strontium titanate and iron titanate, have had little attention [12, 21–23]. Regarding ferric tungstate, several studies on its solid state chemistry have dealt with structural [24–27], magnetic [28, 29] and electrical properties [30–32]. However, little electrochemical information is available in the literature about tungstates in general [30, 33].

It is the purpose of this paper to study the photoelectrochemical properties of ferric tungstate electrodes. This study includes the current-voltage characteristics and the determination of both the band-gap and the flat-band potential of ferric tungstate.

Experimental

Electrode preparation and characterization

Equimolar amounts of α-Fe_2O_3 and WO_3 were mixed by grinding. A sample of 0.2 g of this solid mixture was fused inside a platinum crucible of 3 mm diameter and 1.5 mm depth. Fusion was performed at 1100 °C for 20 min. The fused material was annealed in a stream of oxygen at 800 °C for 10 h and quenched in air to room temperature. Electrical connection to the ferric tungstate electrode was made by soldering the back of the platinum crucible to a copper rod. The crucible and the part of the copper rod to be inserted inside the electrolyte were covered with silicone rubber. The material was identified by X-ray diffraction using a Philips X-ray diffractometer (Model pw 1729) equipped with a copper Kα radiation source. Measurements were undertaken in the range of 2θ 4° to 80 °θ.

Photoelectrochemical measurements

Electrical conductivity was measured by the two-probe technique where the sample was inserted between two tungsten electrodes. A potential of 0.5 V was applied between the two tungsten electrodes and the current was measured at 25 °C by an electrometer.

Experiments were carried out inside a three-electrode electrochemical cell. Ferric tungstate served as the working electrode, a platinum foil of area 1 cm^2 as the counter electrode and a saturated calomel electrode (SCE) as the reference electrode. Current-voltage curves were obtained using an EG & G potentiostat model 273A. Illumination was performed using a 150-W xenon lamp equipped with a monochromator (model QYR-20 from Photochemical Reactor, UK).

The light intensity of the lamp was determined by potassium ferrioxalate actinometry [34]. Adapting this method, a 0.006 M solution of potassium ferrioxalate was irradiated at various wavelengths, and thereby the light intensity of the lamp at each wavelength was determined.

Electrolytes were either 0.1 M NaOH or 0.01 M dimethyl viologen (DMV) in 50 mM phosphate buffer (pH 7) in 0.1 M KNO_3 solution. All reagents used in this study were analytical grade.

Results and discussion

Material characterization

The X-ray powder diffraction pattern for the present electrode material is, as expected, in agreement with that reported for ferric tungstate of the structure Fe_2WO_6 [35].

The d.c. conductivity of Fe_2WO_6 was $4 \times 10^{-6}\ \Omega^{-1}.cm^{-1}$ at 25 °C; therefore this material is a typical semiconductor.

Steady-state photocurrent-voltage curves

Figure 1 illustrates the current-voltage curves of a ferric tungstate electrode in 0.1 M NaOH. Appreciable hysteresis between the forward and reverse sweeps was observed, both in the dark and under illumination. In the forward scan, the current was observed to remain stationary up to 0.8 V (SCE) in the dark, while under illumination it remained stationary up to 0.5 V, and this was followed by an almost exponential increase. This anodic photocurrent requires that the holes in the valence band take part in the transfer reaction. The holes in the valence band suggest that the material is an n-type semiconductor. This is supported by conclusions from the flat-band measurements. Bharati and Singh [31] have reported that Fe_2WO_6 is a p-type semiconductor. However, other studies by Leiva et al. [30] indicated that Fe_2WO_6 an n-type material. The discrepancy between these reports could possibly be due to the wide range of stoichiometry exhibited by this material [36–39].

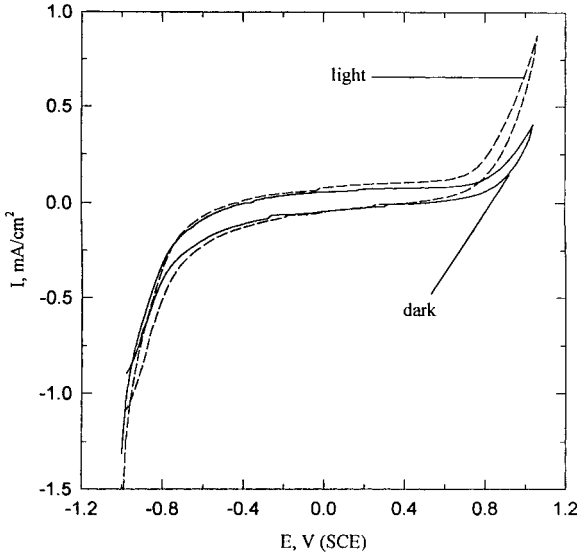

Fig. 1 The current-voltage curves for ferric tungstate electrode under illumination (– – –) and in the dark (———). Electrolyte was 0.1 M NaOH. The sweep rate was 120 mV/S. The light intensity was 1 mW/cm^2 at wavelength 576 nm

Figure 1 shows also that the anodic dark currents are relatively high. Such behavior is unusual for an n-type semiconductor, as the holes which are responsible for this dark current are the minority carriers. This high dark anodic current could be attributed to the existence of a high density of electron-hole recombination centers. In the case of a semiconductor-electrolyte junction, the term recombination centers has been used to describe either traps located in the bulk of the semiconductor or energy levels at the semiconductor/electrolyte interface. Lattice impurities and defects are the main origins for such recombination centers. These centers could act effectively in the process of electron-hole recombination, in which case they become responsible for the generation of low photocurrents and high dark anodic currents.

Another important factor that would increase the dark anodic currents is the corrosion effects. It is possible that the process of electrode preparation could have produced some oxides in which the metal ions have

lower oxidation states e.g., Fe^{2+}. These oxides could be produced during the fusion process by some oxygen loss. As the X-ray diffraction analysis showed the diffraction pattern of $FeWO_6$ only, the concentration of any lower oxides must be very small (<1%). During the anodic scan, these lower oxides would be oxidized in the dark, and therefore the anodic current would be increased.

In the backward direction, the current also increased slowly up to −0.8 V (SCE) in the dark and in the light, and the break-down occurred beyond this potential. The considerably slower increase of current with cathodic voltage is possible only if a large number of energy levels at the surface and deep traps are present in the material, which was the case with our sample.

Figure 2 demonstrates the considerable improvement in the magnitude of the photocurrent brought about by using DMV electrolyte instead of NaOH. This improvement, which was achieved at the expense of an increased cathodic dark current, is attributed to the capability of DMV to introduce surface states through an adsorption process. These states could introduce a new set of levels situated near the valence band, and therefore compete with pre-existing electron-hole recombination centers. Figure 2 also shows strong relaxation effects in the currents. These effects are attributed to the electron-hole recombination process as explained in the next Section.

According to the formalism of the semiconductor/electrolyte band model, the photogenerated current is a result of the appearance of the photogenerated holes at the surface of the semiconductor and the driving of the photogenerated electrons to the Pt electrode. At the semiconductor an oxidation process takes place and at the counter electrode a reduction process. Therefore, the expected redox reaction in the case of NaOH electrolyte is, at the semiconductor electrode

$$2OH^-(aq) + 2h^+ \rightarrow \frac{1}{2}O_2(g) + H_2O(l) \quad (1)$$

and, at the Pt electrode,

$$2H_2O(l) + 2e^- \rightarrow H_2(g) + 2OH^-(aq) \quad (2)$$

The net result of these reactions is the dissociation of water into its components.

In the case of DMV the following redox reactions are expected:

$$V^+(aq) + h^+ \rightarrow V^{2+}(aq) \quad (3)$$

and

$$V^{2+}(aq) + e^- \rightarrow V^+(aq) \quad (4)$$

where V^+ is the radical cation of DMV, which is 1,1′-dimethyl 4,4′-bipyridinium ion, and V^{2+} its dication ion. The redox reaction of DMV is highly reversible, and both the radical cation and the dication are stable in aqueous media [40]. The occurrence of these redox reactions can produce electrical energy. It is the purpose of most of the research carried out in the field of photoelectrochemistry to maximize the efficiency of such redox reactions to make good utilization of solar energy conversion.

Photocurrent behavior under interrupted illumination

Figure 3 shows the photocurrent transients as measured under chopped (576-nm) illumination at 1.0 V (SCE) biasing potential. This photocurrent corresponds to the oxidation of water according to Eq. 1. As the light was turned on, the photocurrent, instead of suddenly increasing to the saturation value, reached about 75% of

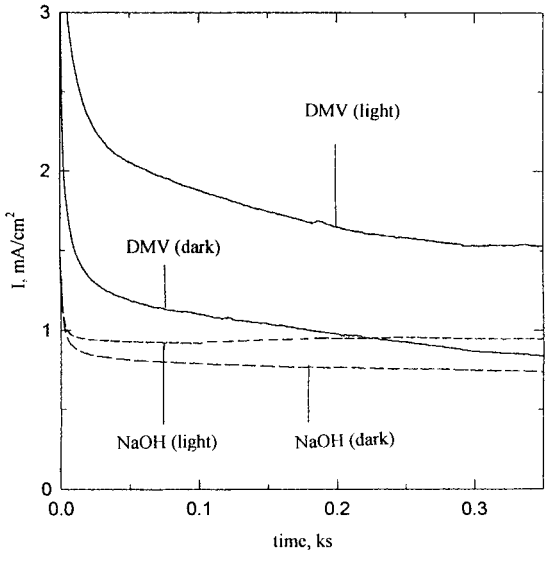

Fig. 2 The photocurrents and the dark currents transients of a ferric tungstate electrode in 0.1 M NaOH and 0.01 M DMV. The electrode was biased at 1.0 V (SCE) and illuminated by 1 mW/cm^2 at 576 nm

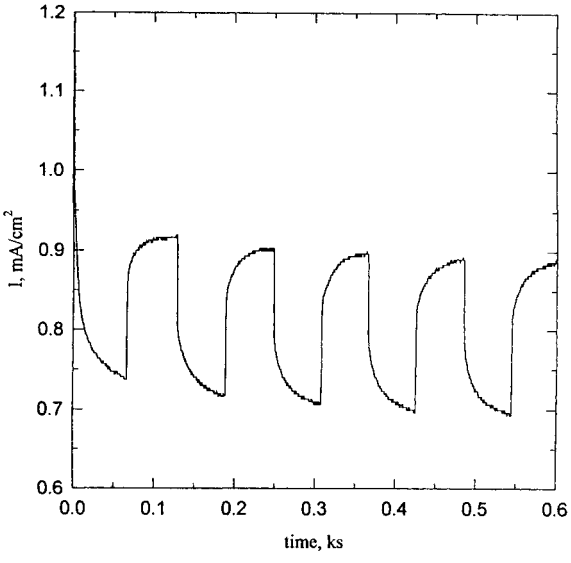

Fig. 3 Photocurrent transient behavior in 0.1 M NaOH at 1.0 V (SCE) under 576-nm interrupted illumination

its saturation value instantaneously, then increased rather nonlinearly during a period of 50 s, until it reached saturation. The difference between the values of the photocurrents in the nonlinear region and the saturation value could be attributed to the back transition of the photogenerated electrons from the conduction band to some levels of lower energy. These levels could be located either deep in the energy gap or at the surface. The origin of such energy levels is usually due to chemical impurities, lattice defects and/or adsorbed species at the surface. The back transition of the photogenerated electrons from the conduction band to the lower energy levels, causing electron-hole recombination, is called carrier relaxation effect. Close examination of the photocurrent in the curved region showed agreement with the exponential form for first-order carrier relaxation, i.e.

$$I_i = I_{oi} \exp(t/\tau_i) \tag{5}$$

where I_i the photocurrent in the curved part during illumination, I_{oi} the value of the photocurrent at the onset time of the process of carrier relaxation and τ_i is the time of recombination between electrons and holes during deexcitation of the photogenerated electrons from the conduction band to lower energy levels. The relationship between the logarithm of the photocurrent and the time is linear as shown in Fig. 4a. The slope of this figure gives a value of 2.5×10^{-3} s for the recombination time. Upon turning the light off, the photocurrent decay transient was quite similar to the current transient observed upon illumination. The relaxation current in this case is described as:

$$I_d = I_{od} \exp(-t/\tau_d) \tag{6}$$

where I_d is the value of the current in the curved part after turning the light off, I_{od} is the preexponential factor, and τ_d is the recombination time associated with transition of an electron from the lower energy levels to the conduction band. The relationship between the logarithm of I_d and the time is also linear as shown in Fig. 4, with a slope τ_d of 3×10^{-3} s. The similarity between τ_i and τ_d signifies that the process of carrier relaxation is reversible.

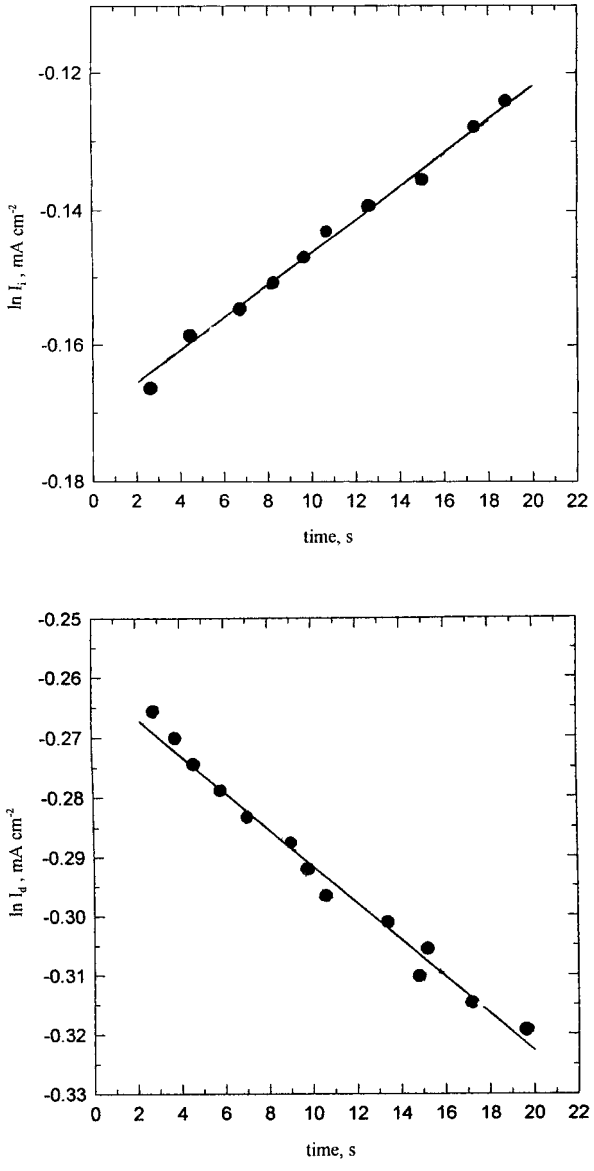

Fig. 4a, b The logarithm of the photocurrent versus time with **a** the light on and **b** the light off. The data were taken from curved parts of the photocurrent transient of Fig. 3

Energy of the band gap

Generally, the semiconductor-electrolyte interface can be treated as a Schottky barrier. Thus according to Ginly and Butler [12, 20], the photocurrent, J, is given by the following relation,

$$J = q\phi_o \left[1 - \exp\left\{ \frac{\left(-\alpha W_o [V - V_{fb}]^{1/2} \right)}{[1 + \alpha L_p]} \right\} \right] \tag{7}$$

were ϕ_o is the photon flux, L_p is the hole diffusion length, V_{fb} is the flat-band potential, W_o is the width of the depletion layer, q is the electronic charge and α is the optical absorption coefficient. Close to the band gap, the optical absorption coefficient, α, is given by:

$$\alpha = A(h\nu - E_g)^{1/2}/h\nu \tag{8}$$

where h is Planck's constant, ν is the frequency of light and E_g the band-gap energy. If the exponential is expanded for $\alpha W_o \ll 1$, then the relationship between $(Jh\nu)^{1/2}$ and $h\nu$ should be linear. This relationship is shown in Fig. 5. The value of the energy gap as determined from the intercept with the abscissa of this figure is ~1.5 eV. This value is in good agreement with the reported value of the energy gap of Fe_2WO_6 [31].

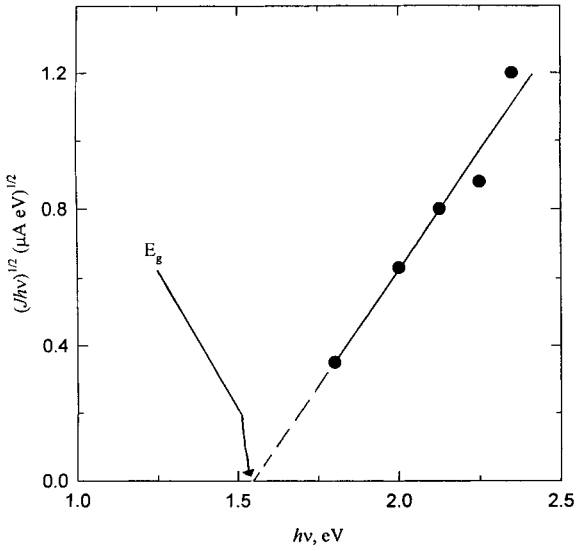

Fig. 5 The photoresponse of Fe_2WO_6 at 1.0 V (SCE) as a function of photon energy. The electrolyte was 0.1 M NaOH. The light intensity was fixed at 1 mW/cm^2 for each light wavelength

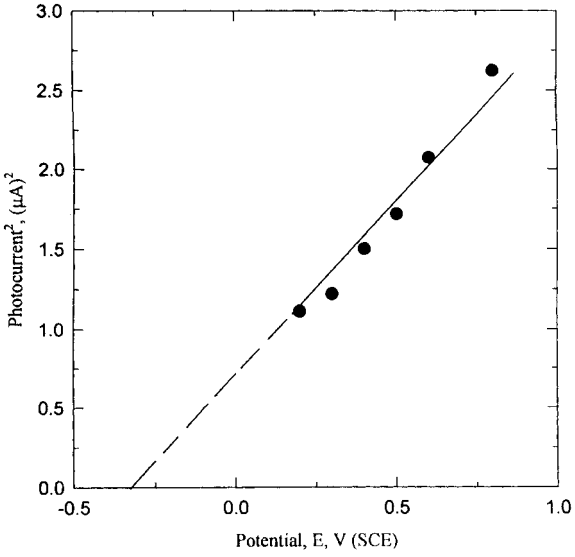

Fig. 6 The square of the photocurrent versus applied potential for an Fe_2WO_6 electrode at 1 mW/cm^2 of 576-nm incident light. The electrolyte was 0.1 M NaOH. The intercept of the straight line with the potential axis is a measure of the flat-band potential (Eq. 9)

Flat-band potential

A simple relationship between the photocurrent and the applied potential was derived by Ginly and Butler [12, 20]. This relationship was obtained by expanding the exponent in Eq. 7 for $\alpha W_o(V-V_{fb})^{1/2} \ll 1$. The relationship between the applied potential and photocurrent becomes:

$$V-V_{fb} \cong (J/\alpha W_o q\phi_o)^2 \quad (9)$$

Therefore the flat-band potential can be determined by extrapolation of the plot of the square of the photocurrent against the applied potential as shown in Fig. 6. The value of V_{fb} is $\cong -0.3$ V (SCE) in 0.1 M NaOH. This value indicates that the energy of the conduction band is not compatible with the hydrogen ion reduction at zero bias, and this process of photodissociation of water would require a high bias for operation.

Conclusions

1. The Fe_2WO_6 is an n-type semiconductor.
2. The photogenerated currents are relatively small, possibly because of the carrier relaxation phenomena.
3. The value of the band-gap energy predicts good utilization of the solar spectrum; however, the process of photoinduced electrolysis of water would require a large applied potential because of the relatively low negative value of the flat-band potential.

References

1. Rao NN, Dube S (1996) Int J Hydrogen Energy 21: 95
2. Iranzo Marin F, Vigneron J, Lincot D, Etcheberry A, Debiemme-chouvy C (1995) J Phys Chem 99: 15198
3. Vanmaekelbergh D, Erne BH, Cheung CW, Tjerkstra RW (1995) Electrochim Acta 40: 689
4. Fujishima A, Nagahara LA, Yoshiki H, Ajito K, Hashimato K (1994) Electrochim Acta 39: 1229
5. Chandra Ababa KS, Pandey RN, Srivastava ON (1995) Int J Hydrogen Energy 20: 771
6. Debeimme-Chouvy C, Fillieres R, Vigneron J, Khoumri EM, Roy DLe, Etcheberry A (1995) Electrochim Acta 40: 89
7. Frese KW, Chem C (1994) J Electrochem Soc 141: 3375
8. Hagio M (1993) J Electrochem Soc 140: 2402
9. Decker F, Soltz DA, Cescato L (1993) Electrochim Acta 38: 95
10. Frank A, Honda K (1982) J Phys Chem 86: 1933
11. Khader MM, Lichtin NN, Vurens GH, Salmeron M, Somorjai GA (1987) J Am Chem Soc 109: 358
12. Ginley DS, Butler MA (1977) J Appl Phys 48: 2019
13. Khader MM (1995) Brit Corrosion J 30: 221
14. Allongue P, Cachet H, Fournier M, Yao NA (1988) Electrochim Acta 33: 693
15. Nakto Y, Ueda K, Tsubomura H (1986) J Phys Chem 90: 5495
16. Schneemeyer LF, Miller B (1982) J Electrochem Soc 129: 1977
17. Inoue T, Watanbe T, Fujishima A, Honda K (1979) Bull Chem Soc Jpn 52: 1243
18. Schaaf N, Hahndorf I, Dohrmann JK (1995) J Electroanal Chem 395: 173
19. Frank SN, Bard AJ (1977) J Am Chem Soc 99: 4667
20. Butler MA (1977) J Appl Phys 48: 1914
21. Pyun SI, Hyun SM (1995) Int J Hydrogen Energy 20: 71
22. Wagner FT, Somorjai GA (1980) J Am Chem Soc 102: 5494
23. Wrighton MS, Ellis AB, Wolczanski PT, Morse DL, Abrahamson HB, Ginley DS (1976) J Am Chem Soc 98: 2774
24. Guskos N, Sadlowski L, Typek J, Likodimos V, Gamari-Seale H, Bojanowski B, Wabia M, Walczake J, Rychlowska-Himmel I (1995) J Solid State Chem 120: 216
25. Walczak J, Rychiowska-Himmel I, Tabero P (1992) J Mater Sci 27: 3680
26. Senegas J, Galy J (1974) J Solid State Chem 10: 5

27. Parant C, Bernier JC, Michel A, Acad CR (1973) Sci Paris Ser C 276: 495
28. Pinto H, Melamud M, Shaked H (1977) Acta Crystallogr Sect A 33: 663
29. Weitzel H (1976) Acta Crystallogr Sect A 32: 592
30. Leiva H, Dwight K, Wold A (1982) J Solid State Chem 42: 41
31. Bharati R, Singh RA (1981) J Mater Sci 16: 511
32. Bharati R, Singh RA,Wanklyn BM (1980) J Mater Sci 15: 1293
33. Arona SK, Mathew T, Batra NM (1990) J Phys D: Appl Phys 23: 460
34. Hatchard CG, Parker CA (1956) Proc R Soc London, Ser A 235: 518
35. Trunov, Kovba (1966) Inorg Mater 2: 127
36. Bharati R, Yadava YP, Singh RA (1983) J Mater Sci Lett 12: 808
37. Sieber K, Leiva H, Kourtakis K, Kershaw R, Dwight K, Wold A (1983) J Solid State Chem 47: 361
38. Harrison WTA, Chowdry U, Machiels CJ, Sleight AW (1985) J Solid State Chem 60: 101
39. Kanachan G, Verma SC, Lal HB (1988) J Mater Sci 23: 924
40. De Lacey AL, Fernandez VM (1995) J Electroanal Chem 399: 163